
Since January 2020 Elsevier has created a COVID-19 resource centre with free information in English and Mandarin on the novel coronavirus COVID-19. The COVID-19 resource centre is hosted on Elsevier Connect, the company's public news and information website.

Informatics in Medicine Unlocked 33 (2022) 101074

Contents lists available at ScienceDirect

Informatics in Medicine Unlocked

journal homepage: www.elsevier.com/locate/imu

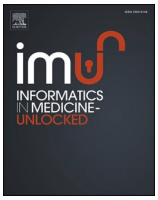

# A computational evaluation of structural stability of omicron and delta mutations of SARS-CoV-2 spike proteins and human ACE-2 interactions

Kehinde A. Idowu *, Collins Onyenaka, Omonike A. Olaleye

*Department of Pharmaceutical and Environmental Health Sciences, College of Pharmacy and Health Sciences, Texas Southern University, 3100 Cleburne St, Houston, TX, 77004, USA*

ARTICLE INFO

*Keywords:*
SARS-CoV-2
Variants delta (B.1.617.2)
Omicron (B.1.1.529)
hACE-2
Molecular interaction

ABSTRACT

Several more infectious SARS-CoV-2 variants have emerged globally since SARS-CoV-2 pandemic and the discovery of the first D614G variant of SARS-CoV-2 spike proteins in 2020. Delta (B.1.617.2) and Omicron (B.1.1.529) variants have proven to be of major concern out of all the reported variants, considering their influence on the virus' transmissibility and severity. This study aimed at evaluating the impact of mutations on these two variants on stability and molecular interactions between the viral Spike protein and human angiotensin converting enzyme-2 (hACE-2). The spike proteins receptor binding domain (RBD) was docked with the hACE-2 using HADDOCK servers. To understand and establish the effects of the mutations on the structural stability and flexibility of the RBD-hACE-2 complex, molecular dynamic (MD) simulation of the docked complex was performed and evaluated. The findings from both molecular docking analysis and binding free energy showed that the Omicron (OM) variant has high receptiveness towards hACE-2 versus Delta variant (DT), thereby, responsible for its increase in transmission. The structural stability and flexibility evaluation of variants' systems showed that mutations on DT and OM variants disturbed the stability of either the spike protein or the RBD-hACE-2 complex, with DT variant having greater instability impact. This study, therefore, assumed this obvious instability observed in DT variant might be associated or responsible for the reported severity in DT variant disease over the OM variant disease. This study provides molecular insight into the effects of OM and DT variants on stability and interactions between SARS-CoV-2 protein and hACE-2.

## 1. Introduction

As of August 24, 2022, about 598, 180, 048 cases of SARS-CoV-2 infections have been recorded (https://coronavirus.jhu.edu/map.html). This huge spread of the virus could be associated with emerging changes/variation in the virus genetic content because of mutation, resulting to emergence of several variants of the virus. Study has shown that the virus RNA, rapidly mutate in host cells [1], thereby produces the diverse variants of the virus. Of the different classifications of SARS-CoV-2 variants by WHO, variants of concern (VOC) have been the most infectious and virulent variants [2]. WHO defined VOC as variants with a) modification in their genetic code that alters SARS-CoV-2 characteristics, b) variants that cause notable viral transmission, and severe COVID-19 epidemiology, and c) reduced drugs/-vaccines efficiency [2].

Presently, five SARS-CoV-2 variants fall under the VOCs, namely, Alpha (lineage B.1.1.7) (Domingo & Benito, 2021), Beta (lineage B.1.351) (Reincke et al., 2022), Gamma (lineage P.1) (Nonaka et al., 2021), Delta (lineage B.1.617.2) [3], and Omicron (lineage B.1.1.529) [4] VOCs. Out of these, Delta (B.1.617.2) and Omicron (B.1.1.529) variants have proven to be of major concern, considering their influence on the virus' transmissibility and severity [5]. Delta variant (lineage B.1.617.2) was discovered in countries within few months and WHO labeled the B.1.617.2 sublineage on May 11, 2021, as a VOC delta variant [6]. By the end of third quarter of 2021, delta variant has become the global dominant VOC [2,4,7]. The predominant mutation in the spike protein of the B.1.617 sublineage includes D614G, L452R, and P681R (Fig. 1 and Table 1). A study by Mlcochova et al. showed that the variant is eight-fold less susceptible to antibodies produced by vaccines and six times less sensitive to serum antibodies from recuperating persons when compared to its wild type [3].

Omicron variant (lineage B.1.1.529) is another VOC. It was detected by the Network for Genomic Surveillance in South Africa on November 24, 2021 [9] and was named by the WHO (WHO, 2021d). The three

* Corresponding author.
*E-mail address:* Kehinde.idowu@tsu.edu (K.A. Idowu).

https://doi.org/10.1016/j.imu.2022.101074
Received 25 July 2022; Received in revised form 31 August 2022; Accepted 1 September 2022
Available online 7 September 2022

sublineages of Omicron include B.1.1.529.1 or (BA.1), B.1.1.529.2 or (BA.2), and B.1.1.529.3 or (BA.3) (Lineage B.1.1.529.2021). Within few months, there has been rapid spread of the viral variant in more than 35 countries around the world [9]. When compared to other VOCs, Omicron's genome was discovered to be a distinctive and predominant variant, thereby causing approximately 55%–60% cases of new SARS-CoV-2 infection cases. It was uncovered to have six distinct mutations which differ from the wild-type (2019 Wuhan variant) resulting to its high transmissibility [10–12] and possible evasion of antibodies.

More than 55 mutations were observed in the genome of the omicron variant. Thirty-one (31) are situated in the S1 domain of the spike glycoprotein [2,13]. 15 of the mutations in the variants situated in the spike protein hACE2 RBD as shown in Fig. 1 and Table 1 [14–16].

This study is focused on the investigation and evaluation of the impact of mutations on these two variants of concerns (Delta and Omicron variant) on the structural stability and flexibility of the RBD-hACE-2, binding affinity and molecular interactions between the viral Spike protein and hACE-2, employing computational techniques. To understand SARS-CoV-2 viral infectivity and pathogenesis, it vital to have better knowledge of the virus' mechanism of recognizing its host receptor (hACE-2). Molecular docking analysis is a widely held and less costly approach to gain understanding of this interaction between SARS-COV-2 and it host receptor, hACE-2. This approach has been employed in several studies that involves computational investigation of either protein-protein or protein-ligands integrations [8,17–20].

## 2. Methods

### 2.1. Proteins acquisition, preparation and molecular docking

The X-ray crystal structures of the complex of SARS-CoV-2 spike glycoprotein with hACE-2 (PDB ID: 7DF4) was obtained from the RSCB Protein Data Bank [21]. The SARS-CoV-2 spike glycoprotein and hACE-2 structures were separated, and the respective mutations for each variant were inserted on the spike protein using rotamer library [22] plugin on the UCSF Chimera software package [23]. The structures of the proteins were prepared by removing water molecules, nonstandard naming, protein residue connectivity. Molecular docking of the structures of Spike RBD for each variant with hACE-2 was done using Haddock molecular docking server [24], with default docking parameters. The docked complexes were then subjected to molecular dynamics simulations.

**Table 1**
Comparism of Spike protein mutations present in Delta and Omicron variants [8].

| | Variants | | |
|---|---|---|---|
| | Wild type (WT) | Delta Variant (B.1.617.2) | Omicron (B.1.1.529) |
| Sequence | NCBI ID: P0DTC2 | NCBI: QWK65230.1 | GSAID ID: R40B60_BHP_3321001247/202 |
| Amino acid/ position of Mutation | – | T19R, G142D, Δ156–157, R158G, Δ213–214, L452R, T478K, D614G, P681R, D950 N | A67V, Δ69–70, T95I, G142D, Δ143–145, N211I, L212V, ins213-214RE, V215P, R216E, G339D, S371L, S373P, S375F, K417 N, N440K, G446S, S477 N, T478K, E484A, Q493R, G496S, Q498R, N501Y, Y505H, T547K, D614G, H655Y, N679K, P681H, N764K, D796Y, N856K, Q954H, N969K, L981F |

### 2.2. Molecular dynamic (MD) simulations

The MD simulation was performed as described by Idowu et al. with little modification [19]. The simulations were performed using the GPU version provided with the AMBER package (AMBER 18) [25], in which the FF18SB variant of the AMBER force field [26] was used to describe the systems.

The Leap module of AMBER 18 allowed for the addition of hydrogen atoms and $Cl^-$ and Na + counter ions to complexes, to neutralize all systems. The systems were then suspended implicitly within an orthorhombic box of TIP3P water molecules such that all atoms were within 10 Å of any box edge [27]. An initial minimization of 2000 steps were carried out with an applied restraint potential of 500 kcal/mol for both solutes. They were performed for 1000 steps using the steepest descent method followed by 1000 steps of conjugate gradients. An additional full minimization of 1000 steps were further carried out using the conjugate gradient algorithm without restraint. A gradual heating MD simulation from 0 K to 300 K was executed for 50 ps, such that the systems maintained a fixed number of atoms and fixed volume. The systems' solutes were imposed with a potential harmonic restraint of 10 kcal/mol and

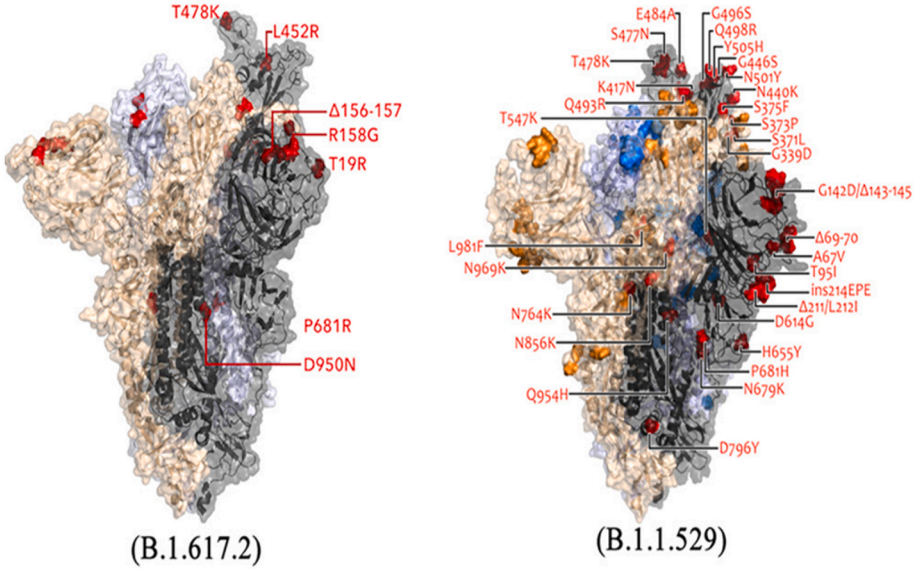


**Fig. 1.** A comparison of Delta and Omicron variant spike mutation [8]. OM spike protein's variation is determined by 30 mutations (3 small deletions and 1 insertion).

collision frequency of 1.0 ps. Following heating, an equilibration estimating 500 ps of each system was conducted; the operating temperature was kept constant at 300 K. Additional features such as several atoms and pressure were also held constant, mimicking an isobaric-isothermal ensemble. The system's pressure was maintained at 1 bar using the Berendsen barostat [28,29].

The total time for the MD simulations conducted was 50 ns. In each simulation, the SHAKE algorithm was employed to constrict hydrogen atoms' bonds [30]. The step size of each simulation was 2fs, and an SPFP precision model was used. The simulations coincided with the isobaric-isothermal ensemble (NPT), with randomized seeding, the constant pressure of 1 bar maintained by the Berendsen barostat [29], a pressure-coupling constant of 2 ps, a temperature of 300 K and Langevin thermostat [31] with a collision frequency of 1.0 ps.

### 2.3. Post-dynamic analysis

Analysis of Root Means Square Deviation (RMSD), Radius of Gyration (RoG), and Solvent Accessible Surface Area (SASA) was done using the CPPTRAJ module employed in the AMBER 18 suit. All raw data plots were generated using python 3.9 on Anaconda3 software.

### 2.4. Binding free energy calculations

To estimate and compare the systems' binding affinity, the free binding energy was calculated using the Molecular Mechanics/GB Surface Area method (MM/GBSA) [32]. Binding free energy was averaged over 50000 snapshots extracted from the 50ns trajectory. The free binding energy (ΔG) computed by this method for each molecular species (complex, ligand, and receptor) can be represented as:

$$\Delta G_{bind} = G_{complex} - G_{receptor} - G_{ligand} \quad (1)$$

$$\Delta G_{bind} = E_{gas} + G_{sol} - TS \quad (2)$$

$$E_{gas} = E_{int} + E_{vdw} + E_{ele} \quad (3)$$

$$G_{sol} = G_{GB} + G_{SA} \quad (4)$$

$$G_{SA} = \gamma SASA \quad (5)$$

$E_{gas}$ denotes the gas-phase energy, which consists of the internal energy $E_{int}$, Coulomb energy $E_{ele}$ and the van der Waals energies $E_{vdw}$. The $E_{gas}$ was directly estimated from the FF14SB force field terms. Solvation free energy, $G_{sol}$, was estimated from the energy contribution from the polar states, $G_{GB}$, and non-polar states, G. The non-polar solvation energy, SA. $G_{SA}$ was determined from the solvent-accessible surface area (SASA), using a water probe radius of 1.4 Å. In contrast, the polar solvation, $G_{GB}$, the contribution was estimated by solving the GB equation. S and T denote the total entropy of the solute and temperature, respectively.

## 3. Results and discussion

In this study, the result of molecular docking analysis of the two variants and wild type of SARS-CoV-2 with hACE-2 showed that the OM variant has highest docking score of −134.4 kcal/mol, while DT variant showed a lower score of −59.2 kcal/mol (Fig. 2). A molecular docking score is therefore a measurement of the fitness of a molecule/ligand into the catalytic active/binding site pocket of an enzyme or protein, and the more negative the value, the better the fitness of the molecule [33]; Shode et al., 2021). This scoring functions allowed the estimation and prediction of the binding affinities of individual molecules [34]. This result corroborates the finding of Kumar et al. that earlier reported OM exhibited highest docking sore of −539.81 kcal/mol, higher than the docking score reported for the DT variant (−529.62 kcal/mol) [8]. Furthermore, the trend in our result is similar to the trend reported in the finding of Hwang et al. that reported docking energy of 340.0 kcal/mol for the WT, 25.2 kcal/mol for the DT, and −382.1 kcal/mol for the OM variant [35]. This indicates that the OM variant is more receptive to the host receptor, hACE2 than the DT. This result might be the first clue to explain the higher infectivity/transmission of SARS-CoV-2 observed in OM variant over the DT variant.

### 3.1. Prediction of the binding energy between variant spike RBD and hACE-2

Molecular dynamics is a popular computational method for calculating the binding affinity and probing energy interaction. In this study, molecular mechanics/generalized born surface area (MMGBSA) computational technique was employed to estimate the binding free energies ($\Delta G_{bind}$) between the variants and wild type spike proteins toward hACE-2. The molecular dynamic simulation of the RBD−hACE-2 docking complexes was used for the predictions of binding affinity between the hACE2 receptor and two variant and WT. Table 2 showed the thermodynamic binding energy profiles for the variants toward hACE-2. The estimated $\Delta G_{bind}$ result showed the binding free energy for RBD and hACE-2 is stronger in OM variant (−43.591 kcal/mol) than the DT variant (−19.743 kcal/mol) and WT- (−29.700 kcal/mol). Our finding is similar to the reports of previous studies that showed the binding affinity

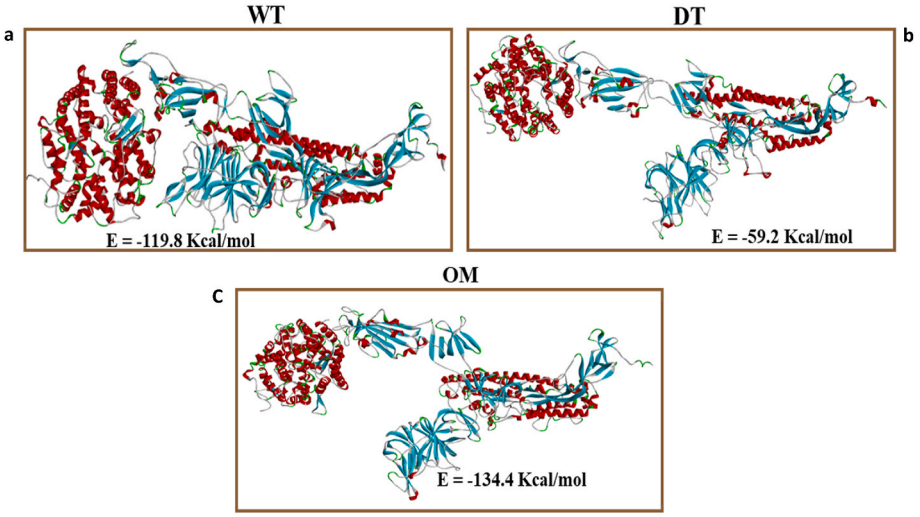


**Fig. 2.** *Molecular Docking scores SARS-CoV-2 Spike glycoprotein Variants* a) Wild-type (WT), b) Delta-type (DT) and c) Omicron type (OM) *toward hACE-2.*

**Table 2**
Thermodynamic Binding Free Energy Profiles for Sgp Variants toward hACE-2.

| Energies | WT | DT | OM |
|---|---|---|---|
| $\Delta E_{vdW}$ | −98.725 ± 6.270 | −57.436 ± 19.141 | −88.452 ± 16.263 |
| $\Delta E_{elec}$ | −951.678 ± 88.028 | −1047.226 ± 63.408 | −1778.178 ± 67.000 |
| $\Delta G_{gas}$ | −1050.403 ± 86.036 | −1104.662 ± 76.974 | −1866.63 ± 74.596 |
| $\Delta G_{solv}$ | 1003.848 ± 87.233 | 1093.919 ± 65.055 | 1836.167 ± 70.992 |
| $\Delta G_{bind}$ | **−29.700 ± 6.383** | **−19.743 ± 5.187** | **−43.591 ± 9.938** |

ΔEele: electrostatic energy, ΔEvdW: van der Waals energy, ΔGsol: solvation free energy, ΔEgas: gas-phase free energy, ΔGbind: total binding free energy.

between hACE-2 and the RBD of the OM variant to be stronger than that of the WT and DT variant [35–37]. For instance, Hwang et al. reported the binding energy was−894.4 kcal/mol for the WT, −980.8 kcal/mol for the DT variant, and −1444.5 kcal/mol for the OM variant [35]. The result of our binding energy together with the molecular docking result, further suggests that the OM variant is more receptive to hACE2 than the DT, and might be associate or responsible for the greater transmission of the virus observed in OM variant than DT variant and WT.

### 3.2. Protein-protein molecular interactions

A typical receptor-ligand interaction examined the molecular interactions between the bound ligand and the amino acid residues at the binding sites of the protein [38,39]; Obakachi et al., 2022). However, in this study we evaluate the protein-protein molecular interactions between the interacting amino acid residues of the spike RBD and the hACE-2. Fig. 3 showed the interaction poses of the RBD-hACE-2 complexes for the variants and WT after 50 ns MD simulation. Table 3 summarized the number and type of interactions that exist within each complex. For the WT complex, a total of 21 interactions (17 hydrogen bonds and 5 hydrophobic bonds) was observed. However, the presence of mutations on the DT spike protein lowers the number of interactions in the DT spike protein-hACE-2 complex to a total of 16 bonds (9 hydrogen and 7 hydrophobic bonds). Furthermore, the DT mutations significantly lower the hydrogen bond in the complex from 17 in WT to 9 in DT. The reduction in interaction, undoubtedly, is responsible for the lowered docking score and binding affinity reported for DT in this study. For the OM variants, insignificant reduction in the number of interactions, 19 (10 hydrogen and 9 hydrophobic bonds) was observed.

However, a significant increase in strong hydrophobic interaction/bond was recorded compared to the WT (5 hydrophobic bond). This study suggests that the increase in the number of strong hydrophobic bonds in OM variant might be the reason for high binding energy and docking score reported in this study and other related studies.

**Table 3**
Interacting Amio residues between the Variants Spike protein and hACE-2.

| WT | DT | OM |
|---|---|---|
| Phe1070-Met64 (Pi-alkyl), Gln6-Ser1061 (Hb), Gly1060-Gln6 (Hb), Tyr65-Ala1059 (Hb), Lys13-Tyr1073 (Pi-sigma), Lys13-Gln1077 (Hb), Lys13-Gln1077 (Hb), Gln1077-Glu17 (Hb), Lys1001-Asp12 (Hb, Salt Bridge), Hie16-Tyr1037 (Pi-pi T-shaped), Tyr1037-Hie16 (Hb), Hie16-Ser1078 (Hb), Arg987-Hie16 (Hb), Tyr1033-Asp20 (Hb), Lys335-Tyr1079 (Hb), Tyr1089-Glu19 (Hb), Tyr1089-Lys335 (Pi-akyl), Tyr23-Gln1082 (Hb), Asn1085-Lys335 (Hb), Gly1086-Lys335 (Hb), Hie16-Ser1078 (Hb, 2.79) | Thr306-Ser1061 (Hb), Asn1071-Ala366 (Hb), Tyr367-Asn1071 (Hb), Ala369-Asn1071 (Hb), Phe338-Ala1059 (Pi-alkyl), Ala368-Ala1059 (Akyl), Gly336-Ala1059 (Hb), Tyr1057-Lys335 (Hb), Phe1040-Lys335 (Pi-alkyl), Lys335-Leu1039 (Hb), Lys335-Leu1039 (Hb), Gln1077-Hie16 (Hb), Lys1001-Asp20 (Hb, Electrostatic), Arg987-Glu17 (Hb; Electrostatic), Lys50-Arg992 (Unfavorable Positive-positive), Arg987-GLU17 (Hb; electrostatic) | Lys1062-Lys335 (Hb), Tyr1073-Ala369 (Hb), Hie16-Leu1039 (pi-alkyl), Arg1077-Glu17 (Hb; electrostatic), Arg1077-Glu17 (Hb; electrostatic), Arg1077-Asp12 (Hb), Arg1077-Asp12 (Hb), Arg1077-Asp12 (Hb), Arg1077-Lys13 (Hb), Lys13-Glu990 (Hb; Electrostatic), Lys13-Glu990 (Hb; Electrostatic), Ser1-Asn1032 (Hb), Ser1-Asn1032 (Hb), Ser1030-Gln6 (Hb), Ser1030-Gln6 (Hb), Arg1082-Tyr65 (Hb; Electrostatic), Tyr1085-Leu61 (Pi-alkyl), Hie1089-Leu61 (Pi-alkyl), Met64-Tyr1085 (Pi-sulfur) |
| **Total = 21 (17 hb, 5 Hydrophobic Bonds)** | **Total = 16 (9 hb, 7 Hydrophobic Bonds)** | **Total 19 (10 Hb, 9 Hydrophobic Bonds)** |

### 3.3. Structural stability and flexibility evaluation of variants' systems

The structural stability of the protein complexes was measured following experimental simulation of the spike protein RBD (for both variants and WT) together with the hACE-2. To confirm the dynamic of the complexes, 50 ns MD simulations was performed. Binding of a molecule (either drugs or protein) to a specific biological target is usually associated with structural and conformational changes, which in

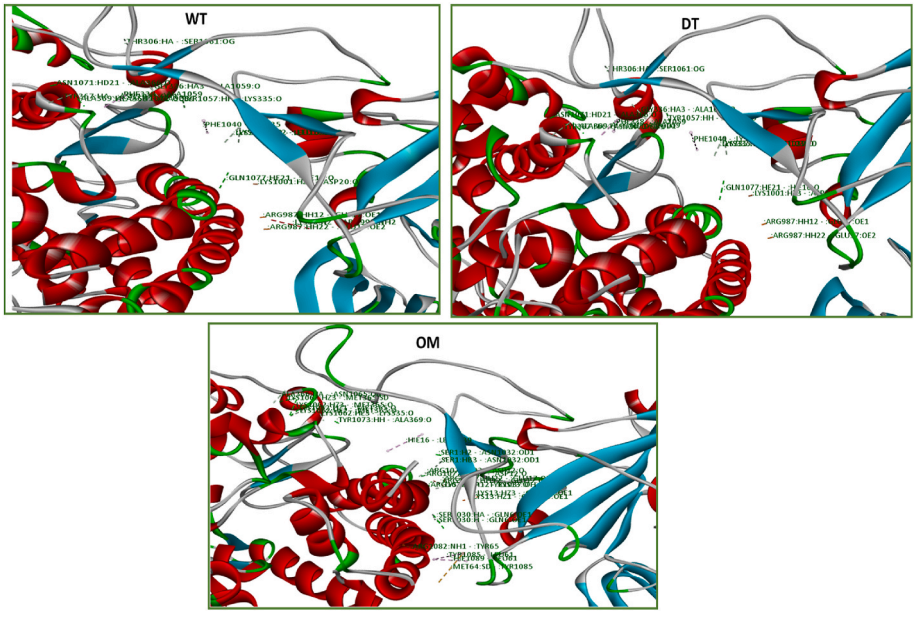


**Fig. 3.** Interacting Amino residues between the Variants' Spike proteins and hACE-2.

most cases influence the biological activity of that target [40–42]. To establish the stability and accurate equilibration of the investigated complexes, RMSD, RoG, RMSF and SASA of alpha carbon (Ca) atoms were monitored and analyzed along with the entire duration of 50 ns of the MD simulation for the WT, DT and OM. These parameters were calculated for the RBD site only (RBD), the whole spike glycoprotein only (SPIKE) and the spike RBD-hACE-2 (RBD-ACE-2) complex.

The measurement of the systems convergence and stability is referred to as RMSD [43]. Figs. 4–6 showed the result of the RMSD plot that measures the complexes' convergence and stability for the RBD, SPIKE and RBD-hACE-2 complex, respectively. Table 4 showed the average values of each parameter used to interpret structural stability of each system. For the RBD (Fig. 4a), the RMSD plot, after maintaining convergence at approximately 8 ns, all the complexes exhibited favorable stability throughout the MD simulations, except for the $RBD_{OM}$ with raised RMSD plot at 28 ns. The average RMSD value for $RBD_{OM}$ (2.95 Å) is higher that the estimated values for $RBD_{DT}$ and $RBD_{WT}$ with average values of 2.54 Å and 2.47 Å, respectively (Table 4). The mutations on the OM variant increase the RMSD plot, thereby altering its stability. However, for the whole spike systems, after all the systems maintained convergence at approximately 5 ns, $SPIKE_{OM}$ and $SPIKE_{DT}$ systems exhibited unfavorable stability throughout the MD simulations (Fig. 5a). With the DT variant showing the highest average RMSD value of 8.95 Å, and $SPIKE_{OM}$ exhibited the lowest value of 7.28 Å. A similar trend was observed in the RBD-

ACE-2 complexes, where the RBD-ACE-$2_{DT}$ showed the highest instability as evidenced by its high average RMSD value of 10.58 Å compared to the RBD-ACE-$2_{WT}$ and SPIKE-ACE-$2_{OM}$ complexes with average RMSD of values of 9.23 Å and 7.81 Å, respectively (Fig. 6a). The RMSD plots of the RBD, SPIKE and RBD-ACE-2 showed that both OM and DT mutations affect the stability of the protein but, with the DT variant exhibiting pronounced instability in its protein complexes.

To understand the compactness of the alpha carbon backbones of the protein complexes, the RoG values for each complex were examined. The RoG value is a measure of the extent of compactness of the alpha carbon backbones of the proteins. An increase in RoG values implies a decrease in protein structure compactness, thereby suggesting decreased stability [44]. Figs. 4b, 5b and 6b showed the RoG plots for all the RBD, SPIKE and RBD-ACE-2 systems, respectively and Table 4, showed the average RoG values for all the systems. The result revealed that RoG plots of $RBD_{DT}$ and $RBD_{OM}$ exhibited decrease in structural compactness suggesting high mobility and less stability as evidenced by the higher average RoG values of 18.75 Å and 18.57 Å for $RBD_{DT}$ and $RBD_{OM}$, respectively when compared to the $RBD_{WT}$ (18.43 Å). For the whole spike (SPIKE) systems, a similar trend was observed. The RoG plots of.

$SPIKE_{DT}$ and $SPIKE_{OM}$ demonstrated decline in structural compactness suggestive of high mobility and less stability as supported by the higher average RoG values of 47.69 Å and 45.16 Å for $SPIKE_{DT}$ and $SPIKE_{OM}$, respectively when compared to the $SPIKE_{WT}$ (44.93 Å). Likewise, just as observed in both RBD and SPIKE systems, the estimated RoG plots of RBD-ACE-$2_{DT}$ and RBD-ACE-$2_{OM}$ also demonstrated decline in structural compactness indicative of high mobility and less stability as evidenced by the higher average RoG values of 60.94 Å and 60.58 Å for RBD-ACE-$2_{DT}$ and RBD-ACE-$2_{OM}$, respectively when compared to the RBD-ACE-$2_{WT}$ (58.41 Å). The results of the RoG plots of the RBD, SPIKE and RBD-ACE-2 showed that both OM and DT mutations disturb the stability of the interaction between hACE-2 and RBD, however, the DT mutations exhibit more obvious instability in its protein complexes than the OM mutations.

Figs. 4c, 5c and 6c showed the RMSF plots for all the RBD, SPIKE and RBD-ACE-2 systems, respectively and Table 4, showed the average RMSF values for all the systems. RMSF is a measure of the impacts of the binding of molecule on the behavior of the active residue [45]. And high RMSF values indicated increase flexible movements, and in contrast, lower values meant restricted fluctuations. For the RBD systems (Fig. 4c), $RBD_{DT}$ and $RBD_{OM}$ showed higher flexible movements as evidenced by higher overall average values of 18.75 Å and 18.57 Å, compared to the $RBD_{WT}$. Nevertheless, at amino acid residues 1060–1070 (the residues on RBD involved in interaction with hACE-2), all the RBD systems showed a noticeable increase in fluctuation, with the $RBD_{OM}$ exhibiting more flexibility than others. This finding is suggestive of how much activity and flexibility required of the interacting amino acid residues in interacting with hACE-2. A look at the whole spike structure, we observed the $SPIKE_{DT}$ exhibited higher fluctuation (7.49 Å) than both the $SPIKE_{WT}$ and $SPIKE_{OM}$. This finding further corroborates our previous findings that showed that the DT mutations mostly disturbed the protein stability than the $SPIKE_{OM}$ mutations. Similarly, the both the RBD-hACE-$2_{DT}$ (9.66 Å) and RBD-hACE-$2_{OM}$ (7.05 Å) induces more flexible movements on the amino acid residues, with both variants showing higher flexibility than the RBD-hACE-$2_{WT}$ (6.11 Å).

To measures the proteins exposure to solvent molecules, the SASA plots for all the systems were examined (Figs. 4–6). A high SASA value

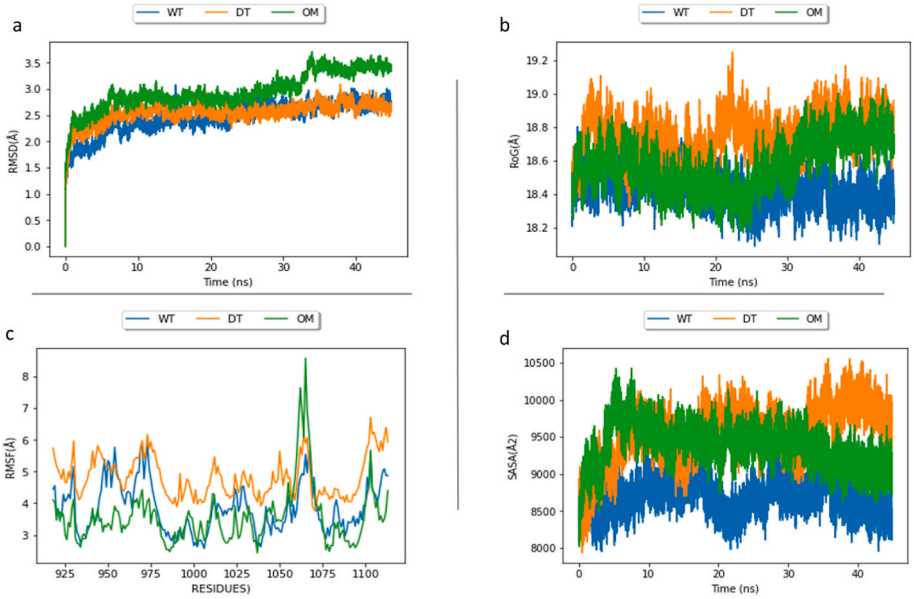


**Fig. 4.** Comparative a). RMSD b). RoG c). RMSF, and d). SASA profile plots of C-a atoms of RBD calculated throughout 50 ns molecular dynamics simulation.

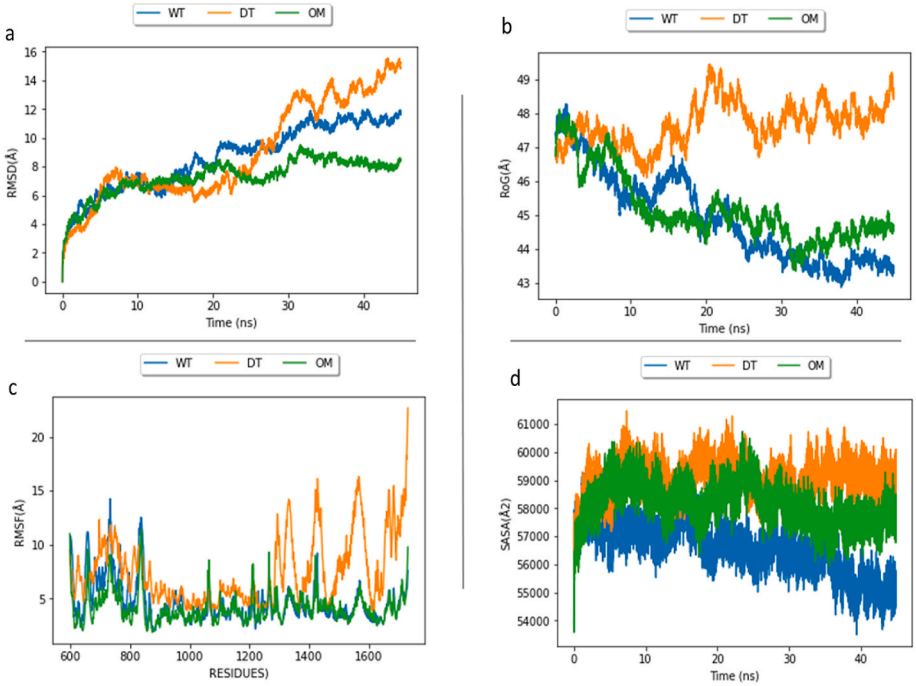


**Fig. 5.** Comparative a). RMSD b). RoG c). RMSF, and d). SASA profile plots of C-a atoms of Whole Spike proteins calculated throughout 50 ns molecular dynamics simulation.

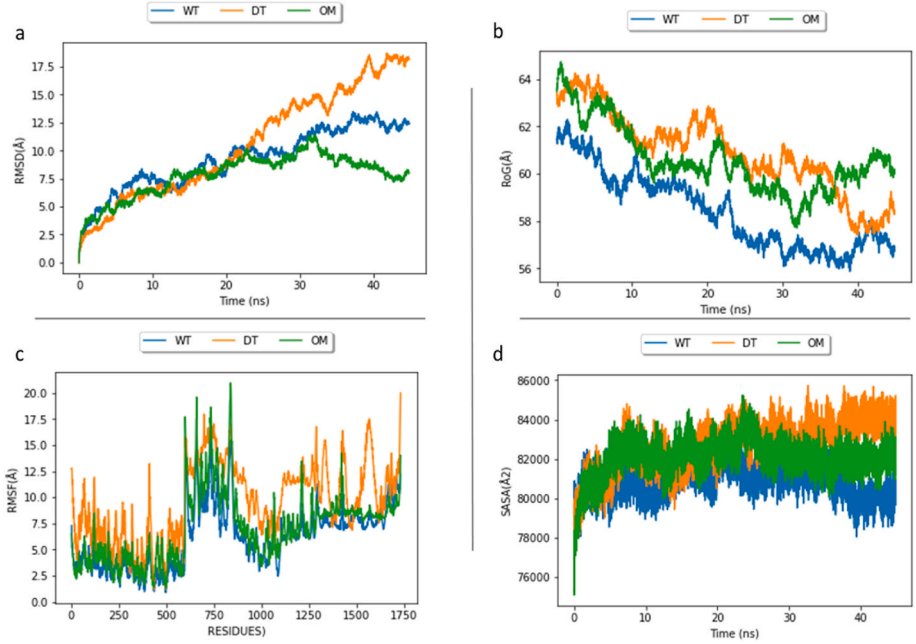


**Fig. 6.** Comparative a). RMSD b). RoG c). RMSF, and d). SASA profile plots of C-a atoms of Spike-hACE-2 complex calculated throughout 50 ns molecular dynamics simulation.

has been reported to be an indication of decrease in the exposure of buried hydrophobic residues which suggest decrease in systems stability [46,47]. The result of average SASA values for the systems (Table 4), showed both $RBD_{OM}$ and $RBD_{DT}$ increase the SASA plots and average values far higher than the $RBD_{WT}$. This finding indicates that both $RBD_{OM}$ and $RBD_{DT}$ decreased the exposure of buried hydrophobic residues which means decrease in the RBD stability. Likewise, in the whole spike complexes, the two variants decreased the SPIKE stability as proven by high SASA values of 59078 $Å^2$ ($SPIKE_{DT}$) and 58152 $Å^2$ ($SPIKE_{OM}$) compared to the $SPIKE_{WT}$ (56596 $Å^2$). Equally, as reported in both the RBD and SPIKE systems, in the RBD-hACE-2 systems the RBD-$hACE\text{-}2_{OM}$ (82051 $Å^2$) and RBD-$hACE\text{-}2_{DT}$ (82721 $Å^2$) increase the SASA average values far higher than the $RBD_{WT}$, which indicates that both $RBD_{OM}$ and $RBD_{DT}$ decreased the exposure of buried hydrophobic residues which mean decrease in the RBD-hACE-2 complex stability.

The findings of this study from all the structural stability parameters uniformly showed that mutations from both DT and OM variants disturbed the stability of either the spike protein or the RBD-hACE-2 complex. From the examination of the mutations present on the RDBs of the two variants; OM (G339D, S371L, S373P, S375F, K417 N, N440K,

**Table 4**
Calculated Average Values of Parameter used to Interpret Structural stability and Flexibility of Variants' Systems.

| Parameters | RBD | | | Spike Protein | | | Spike-hACE-2 | | |
|---|---|---|---|---|---|---|---|---|---|
| | WT | DT | OM | WT | DT | OM | WT | DT | OM |
| **RMSD** | 2.47 ± 0.30 | 2.54 ± 0.20 | 2.95 ± 0.35 | 8.75 ± 2.30 | 8.95 ± 3.46 | 7.28 ± 1.26 | 9.23 ± 2.60 | 10.58 ± 4.81 | 7.81 ± 1.88 |
| **RMSF** | 3.85 ± 0.77 | 4.82 ± 0.63 | 3.56 ± 0.89 | 4.62 ± 1.95 | 7.49 ± 3.10 | 4.12 ± 1.37 | 6.11 ± 2.90 | 9.66 ± 3.74 | 7.05 ± 3.32 |
| **ROG** | 18.43 ± 0.10 | 18.75 ± 0.13 | 18.57 ± 0.14 | 44.93 ± 1.32 | 47.69 ± 0.63 | 45.16 ± 1.00 | 58.41 ± 1.62 | 60.94 ± 1.71 | 60.58 ± 1.41 |
| **SASA** | 8680.43 ± 213.87 | 9548.53 ± 376.15 | 9372.75 ± 285.18 | 56596 ± 906.08 | 59078.34 ± 604.38 | 58152.34 ± 731.50 | 80911.81 ± 773.16 | 82721.99 ± 1209 | 82051.91 ± 921.76 |

G446S, S477 N, T478K, E484A, Q493R, G496S, Q498R, N501Y, Y505H) and DT (L452R, T478K), it could be inferred that the presence of 15 mutations on OM RBD increases its affinity to hACE-2. Only mutation T478K is common to both variants RBD. Furthermore, the study reveal instability impact of the mutations on DT variant is more pronounced than the OM variant as evidenced by higher average values of structural stability plots and average values. This study, therefore, assumed this obvious instability observed in DT variant might be associated or responsible for the reported severity in DT variant disease than the OM variant disease [48,49]. Furthermore, this study believes, as shown in our result (binding energy together with the molecular docking results), that high transmission of the OM variants is associated with higher receptiveness reported to exist between OM spike protein and hACE2.

## 4. Conclusion

After the emergence of Severe Acute Respiratory Syndrome Coronavirus type 2 (SARS-CoV-2), variants Delta (B.1.617.2) and Omicron (B.1.1.529) have proven to be of major concern out of all the reported variants, considering their influence on the virus' transmissibility and severity. Mutations on the variants' spike protein have either increase the disease transmissibility or severity. Therefore, this study evaluates the impact of mutations on these two variants on stability and molecular interactions between the viral Spike protein and hACE-2. The findings of this study showed the OM variant has high receptiveness towards hACE-2, thereby, increase its transmission. The study further showed that DT and OM variants disturbed the stability of either the spike protein or the RBD-hACE-2 complex, with DT variant having more instability impact. This study provides molecular dynamic insight into the effects of OM and DT variants on the stability and molecular interactions between SARS-CoV-2 Spike protein and hACE-2.

Evaluation of a monomer of Spike protein instead of trimers over a molecular dynamic simulation period of 50 ns is the only limitation to this study. This is because molecular dynamic simulation of complex structures of protein-protein interactions is relatively difficult. However, this is not expected to change or affect the findings of this study. Furthermore, similar studies have also worked on spike protein monomers.

## Funding source

This project is sponsored by the NIH-RCMI (U54MD007605) and CPRIT-CTTP (RP210043) Grants.

## Declaration of competing interest

The authors declare that they have no known competing financial interests or personal relationships that could have appeared to influence the work reported in this paper.

## References

[1] Ganeshpurkar A, Gutti G, Singh SK. RNA-dependent RNA polymerases and their emerging roles in antiviral therapy. In: Viral polymerases: structures, functions and roles as antiviral drug targets. Elsevier; 2018. p. 1–42. https://doi.org/10.1016/B978-0-12-815422-9.00001-2.

[2] World Health Organization. easy-to-say labels for SARS-CoV-2 variants of interest and concern. Retrieved from, https://www.who.int/news/item/31-05-2021-who-announces-simple-easy-to-saylabels-for-sars-cov-2-variants-of-interest-and-concern; 2021.

[3] Mlcochova P, Kemp S, Dhar MS, Papa G, Meng B, Ferreira IATM, Gupta RK. SARS-CoV-2 B.1.617.2 Delta variant replication and immune evasion. Nature 2021. https://doi.org/10.1038/s41586-021-03944-y.

[4] World Health Organizations. Classification of omicron (B.1.1.529): world health organizations (2021). SARS-CoV-2 variant of concern. 2021. Retrieved from, https://www.who.int/news/item/26-11-2021-classification-of-omicron-(b.1.1.529)-sars-cov-2-variant-of-concern.

[5] World Health Organizations. Tracking SARS-CoV-2 variants. 2022. Retrieved from, https://www.who.int/en/activities/tracking-SARS-CoV-2-variants/.

[6] Public Health England. SARS-CoV-2 variants of concern and variants under investigation in England. Sage; 2021. p. 1–50. April.

[7] World Health Organization. Classification of omicron (B.1.1.529). T. A. G. on S.-C.-2 V. E. (TAG-V. 2021. SARS-CoV-2 Variant of Concern. Retrieved from, https://www.who.int/news/item/26-11-2021-classification-of-omicron-(b.1.1.529)-sars-cov-2-variant-of-concern.

[8] Kumar S, Thiviya ST, Kalimuthu K, Gunasekaran S. Omicron and Delta variant of SARS-CoV-2: a comparative computational study of spike protein. J Med Virol 2021;94(2022):1641–9. https://doi.org/10.1002/jmv.27526.

[9] Gowrisankar A, Priyanka T, Banerjee S. Omicron: a mysterious variant of concern. Europ. phy. j. plus 2022;137(1):100. https://doi.org/10.1140/epjp/s13360-021-02321-y.

[10] Pulliam J, van Schalkwyk C, Govender N, von Gottberg A, Cohen C, Groome MJ, Dushoff J, Mlisana K, Moultrie H. Increased risk of SARS-CoV-2 reinfection associated with emergence of Omicron in South Africa. Science 2022. https://doi.org/10.1126/science.abn4947. New York, N.Y.), eabn4947. Advance online publication.

[11] Brandal LT, MacDonald E, Veneti L, Ravlo T, Lange H, Naseer U, Feruglio S, Bragstad K, Hungnes O, Ødeskaug LE, Hagen F, Hanch-Hansen KE, Lind A, Watle SV, Taxt AM, Johansen M, Vold L, Aavitsland P, Nygård K, Madslien EH. Outbreak caused by the SARS-CoV-2 omicron variant in Norway, november to december 2021. Euro Surveill: bullet. Europ. sur les malad. transmis = Europ. commun. dis. bullet. 2021;26(50):2101147. https://doi.org/10.2807/1560-7917.ES.2021.26.50.2101147.

[12] Espenhain L, Funk T, Overvad M, Edslev SM, Fonager J, Ingham AC, Rasmussen M, Madsen SL, Espersen CH, Sieber RN, Stegger M, Gunalan V, Wilkowski B, Larsen NB, Legarth R, Cohen AS, Nielsen F, Lam J, Lavik KE, Karakis M, Müller L. Epidemiological characterisation of the first 785 SARS-CoV-2 Omicron variant cases in Denmark, December 2021. Euro Surveill: bullet. Europ. sur les malad. transmis = Europ. commun. dis. bullet. 2021;26(50):2101146. https://doi.org/10.2807/1560-7917.ES.2021.26.50.2101146.

[13] Lupala CS, Ye Y, Chen H, Su XD, Liu H. Mutations on RBD of SARS-CoV-2 Omicron variant result in stronger binding to human ACE2 receptor. Biochem Biophys Res Commun 2022;590:34–41. https://doi.org/10.1016/j.bbrc.2021.12.079.

[14] Elbe S, Buckland-Merrett G. Data, disease, and diplomacy: GISAID's innovative contribution to global health. Glob. challeng. (Hoboken, NJ) 2017;1(1):33–46. https://doi.org/10.1002/gch2.1018.

[15] Cerutti G, Guo Y, Liu L, Liu L, Zhang Z, Luo Y, Huang Y, Wang HH, Ho DD, Sheng Z, Shapiro L. Cryo-EM structure of the SARS-CoV-2 Omicron spike. Cell Rep 2022;38(9):110428. https://doi.org/10.1016/j.celrep.2022.110428.

[16] Cui Z, Liu P, Wang N, Wang L, Fan K, Zhu Q, Wang K, Chen R, Feng R, Jia Z, Yang M, Xu G, Zhu B, Fu W, Chu T, Feng L, Wang Y, Pei X, Yang P, Xie XS, Wang X. Structural and functional characterizations of infectivity and immune evasion of SARS-CoV-2 Omicron. Cell 2022;185(5):860–71. https://doi.org/10.1016/j.cell.2022.01.019. e13.

[17] Sabiu Saheed, Idowu K. An insight on the nature of biochemical interactions between glycyrrhizin, myricetin and CYP3A4 isoform. J Food Biochem 2021;2(3):232–43. https://doi.org/10.1111/jfbc.13831.

[18] Uhomoibhi JO, Shode FO, Kehinde Ademola I, Sabiu S. Molecular modelling identification of phytocompounds from selected African botanicals as promising therapeutics against druggable human host cell targets of SARS-CoV-2. J Mol Graph Model 2022. https://doi.org/10.1016/j.jmgm.2022.108185.

[19] Idowu AK, Egbejimi A, Kaur M, Onyenaka C, Adebusuyi T, Olaleye OA. Inhibitory mechanism of ambroxol and bromhexine hydrochlorides as potent blockers of molecular interaction between SARS-CoV-2 spike protein and human angiotensin-converting enzyme-2. J Mol Graphic and dyn 2022.

[20] Obakachi, V. A., Idowu, K, Narva Deshwar Kushwaha, Olayinka I. Akinpelu, Babita Kushwaha, Srinivas Reddy Merugu, Rajshekhar Karpoormath. "Structural based investigation of novel pyrazole-thiazole hybrids as dual CDK-1 and CDK-2 inhibitors for cancer chemotherapy" molecular simulation, DOI: 10.1080/08927022.2022.2045016.

[21] Xu C, Wang Y, Liu C, Zhang C, Han W, Hong X, Wang Y, Hong Q, Wang S, Zhao Q, Wang Y, Yang Y, Chen K, Zheng W, Kong L, Wang F, Zuo Q, Huang Z, Cong Y. Conformational dynamics of SARS-CoV-2 trimeric spike glycoprotein in complex with receptor ACE2 revealed by cryo-EM. Sci Adv 2021;7. https://doi.org/10.1126/sciadv.abe5575.

[22] Shapovalov MV, Dunbrack Jr RL. A smoothed backbone-dependent rotamer library for proteins derived from adaptive kernel density estimates and regressions. 1993 Structure (London, England 2011;19(6):844–58. https://doi.org/10.1016/j.str.2011.03.019.

[23] Yang Z, Lasker K, Schneidman-Duhovny D, Webb B, Huang CC, Pettersen EF, Goddard TD, Meng EC, Sali A, Ferrin TE. UCSF chimera, MODELLER, and IMP: an integrated modeling system. J Struct Biol 2012;179(3):269–78.

[24] Dominguez CR, Alexandre MJJ. HADDOCK: a protein-protein docking approach based on biochemical or biophysical information. J Am Chem Soc 2003 2003;125(7):1731–7.

[25] Case DA, H M, Aktulga K, Belfon IY, Ben-Shalom SR, Brozell DS, Cerutti TE, Cheatham III, Cisneros GA, Cruzeiro VWD, Darden TA, Duke RE, Giambasu G, Gilson MK, Gohlke H, Goetz AW, Harris R, Izadi S, Izmailov SA, Jin C, Kasavajhala K, Kaymak MC, King E, Kovalenko A, Kurtzman T, Lee TS, LeGrand S, Li P, Lin C, Liu J, Luchko T, Luo R, Machado M, Man V, Manathunga M, Merz KM, Miao Y, Mikhailovskii O, Monard G, Nguyen H, O'Hearn KA, Onufriev A, Pan F, Pantano S, Qi R, Rahnamoun A, Roe DR, Roitberg A, Sagui C, Schott-Verdugo S, Shen J, Simmerling CL, Skrynnikov NR, Smith J, Swails J, Walker RC, Wang J, Wei H, Wolf RM, Wu X, Xue Y, York DM, Zhao S, Kollman PA. Amber 2021. San Francisco: University of California; 2021.

[26] Nair PC, Miners JO. Molecular dynamics simulations: from structure function relationships to drug discovery. Silico Pharm 2014;2(1):1–4. https://doi.org/10.1186/s40203-014-0004-8.

[27] Jorgensen WL, Chandrasekhar J, Madura JD, Impey RW, Klein ML. Comparison of simple potential functions for simulating liquid water. J Chem Phys 1983;79(2):926–35.

[28] Gonnet P. P-SHAKE: a quadratically convergent SHAKE in O(n2). J Comput Phys 2007;220(2):740–50. https://doi.org/10.1016/j.jcp.2006.05.032.

[29] Basconi JE, Shirts MR. Effects of temperature control algorithms on transport properties and kinetics in molecular dynamics simulations. J Chem Theor Comput 2013;9(7):2887–99. https://doi.org/10.1021/ct400109a.

[30] Ryckaert JP, Ciccotti G, Berendsen HJ. Numerical integration of the Cartesian equations of motion of a system with constraints: molecular dynamics of n-alkanes. J Comput Phys 1977;23(3):327–41. https://doi.org/10.1016/0021-9991(77)90098-5.

[31] Izaguirre JA, Catarello DP, Wozniak JM, Skeel RD. Langevin stabilization of molecular dynamics. J Chem Phys 2001;114(5):2090–8. https://doi.org/10.1063/1.1332996.

[32] Ylilauri M, Pentik€ainen OT. MMGBSA as a tool to understand the binding affinities of filamin-peptide interactions. J Chem Inf Model 2013;53(10):2626–33.

[33] Idowu K, Ramharack P, Nlooto M, Gordon M. Molecular dynamic mechanism(s) of inhibition of bioactive antiviral phytochemical compounds targeting cytochrome P450 3A4 and P-glycoprotein. J Biomol Struct Dyn 2020:1–11. https://doi.org/10.1080/07391102.2020.1821780.

[34] Abdullahi M, Olotu FA, Soliman ME. Allosteric inhibition abrogates dysregulated LFA-1 activation: structural insight into mechanisms of diminished immunologic disease. Comput Biol Chem 2018;73:49–56. https://doi.org/10.1016/j.compbiolchem. 2018.02.002.

[35] Hwang S, Baek S, Park D. Interaction analysis of the spike protein of delta and omicron variants of SARS-CoV-2 with hACE2 and eight monoclonal antibodies using the fragment molecular orbital method. J Chem Inf Model 2022 2022;62:1771–82.

[36] Lan J, He X, Ren Y, Wang Z, Zhou H, Fan S, Zhu C, Liu D, Shao B, Liu T-Y, Wang Q, Zhang L, Ge J, Wang T, Wang X. Structural and computational insights into the SARS-CoV2 omicron RBD-ACE2 interaction. bioRxiv 2022. https://doi.org/10.1101/2022.01.03.474855.

[37] Costa CH, Freitas CA, Alves CN. Assessment of mutations on RBD in the spike protein of SARS-CoV-2 alpha, delta and omicron variants. Research Square 2022. https://doi.org/10.21203/rs.3.rs-1401835/v1.

[38] Kehinde I, Ramharack P, Nlooto M, Gordon M. The pharmacokinetic properties of HIV-1 protease inhibitors: a computational perspective on herbal phytochemicals. Heliyon 2019;5(10):e02565. 10.1016/j.

[39] Vincent OA, Kushwaha ND, Kushwaha B, Mavela CM, Srinivas RM, Idowu KA, Rajshekhar K. Design and synthesis of pyrazolone-based compounds as potent blockers of SARS-CoV-2 viral entry into the host cells. J Mol Struct 2021;1241:130665. https://doi.org/10.1016/j.molstruc.2021.130665.

[40] Sindhu T, Srinivasan P. Exploring the binding properties of agonists interacting with human TGR5 using structural modelling, molecular docking and dynamics simulations. RSC Adv 2015;5(19):14202–13. https://doi.org/10.1039/C4RA16617E.

[41] Aribisala JO, Nkosi Sonto, Kehinde Idowu, Nurain Ismalia, Shode FO, Saheed Sabiu. Astaxanthin-mediated bacterial lethality: evidence from oxidative stress contribution and molecular dynamics simulation. Oxid Med Cell Longev 2021. https://doi.org/10.1155/2021/7159652.

[42] John OU, Kehinde AI, Shode OF, Saheed S. Molecular modelling identification of potential drug candidates from selected African plants against SARS-CoV-2 key druggable proteins. Scientific African 2022.

[43] Hess B. Convergence of sampling in protein simulations. Phys Rev 2002;65(3):31910.

[44] Idowu AK, Egbeyemi Anu, Kaur Manvir, Onyenaka Collins, Adebusuyi Tolulope, Olaleye Omonike A. Inhibitory mechanism of clioquinol and its derivatives at the exopeptidase site of human angiotensin-converting enzyme-2 and receptor binding domain of SARS-CoV-2 viral spike protein. J Biomol Struct Dyn 2022. https://doi.org/10.1080/07391102.2022.2043938.

[45] Kumar CV, Swetha RG, Anbarasu A, Ramaiah S. Computational analysis reveals the association of threonine 118 methionine mutation in PMP22 resulting in CMT-1A". Advan. Bioinformatics 2014;2014:1–10.

[46] Ogidigo JO, Emmanuel AI, Ibeji CU, Okpalefe O, Soliman MES. Natural phyto, compounds as possible noncovalent inhibitors against SARS-CoV2 protease: computational approach. https://doi.org/10.1080/07391102.2020.1837681; 2020.

[47] Sinyani A, Idowu K, Shunmugam L, Kumalo HM, Khan Rene. A molecular dynamics perspective into estrogen receptor inhibition by selective flavonoids as alternative therapeutic options. J Biomol Struct Dyn 2022. https://doi.org/10.1080/07391102.2022.2062786.

[48] Joseph A Lewnard, Hong Vennis X, Patel Manish M, Kahn Rebecca, Lipsitch Marc, Sara YT. Clinical outcomes among patients infected with Omicron (B.1.1.529) SARS-CoV-2 variant in southern California. 2022. https://doi.org/10.1101/2022.01.11.22269045.

[49] Lindsey W, Berger Nathan A, David C, Kaelber, Pamela B, Davis, Nora D, Volkow, Xu Rong. Comparison of outcomes from COVID infection in pediatric and adult patients before and after the emergence of Omicron. https://doi.org/10.1101/2021.12.30.21268495; 2022.